AIChE

Identification of Multiscale Nature and Multiple Dynamics of the Blast Furnace System from Operating Data

Chuanhou Gao and Jiusun Zeng
Dept. of Mathematics, Zhejiang University, Hangzhou 310027, P.R. China

Zhimin Zhou
College of Mathematics and Statistics, Zhejiang University of Finance & Economics, 310018 Hangzhou, P.R. China

DOI 10.1002/aic.12554
Published online March 10, 2011 in Wiley Online Library (wileyonlinelibrary.com).

Very often, there are several kinds of different scale structures, such as atomic/molecular microscale, device/boundary mesoscale and working procedure/operation unit macroscale, etc., referred in the operation of a blast furnace system. However, not enough attention has been paid to the multiscale feature of the blast furnace system by traditional analytic methods which are the average ones over a fixed scale. For this reason, the current work performs a multiscale identification and further makes a dynamical analysis on the blast furnace system from the time series sets of two important components in the blast furnace hot metal, i.e., silicon content and sulfur content, collected from a pint-sized blast furnace. The results render a strong indication of multiscale characteristic and multiple dynamics, i.e., randomicity, chaos, and limit cycle but with different rates of contribution to the whole system, contained in the blast furnace system. Furthermore, compared with the original blast furnace system, every subscale structure has lower complexity. All of these can serve as guidelines to carry out modeling, control and optimization on complex blast furnace system from the viewpoint of multiscale in the future, and may throw more light on understanding and characterizing its complex dynamics. © 2011 American Institute of Chemical Engineers *AIChE J,* 57: 3448–3458, 2011
Keywords: blast furnace system, multiscale, dynamics, time series

Introduction

The modeling and control of complex blast furnace system is one of the oldest puzzles in contemporary metallurgical engineering both theoretically and experimentally and will continue to constitute an active research issue of the operation of the blast furnace in the foreseeable future. The key reason is that steel industry plays a major role on national economy, and a slight improvement may produce considerable economic gains. Recently, with fast growing demand for steel in industry and society plus strongly rising prices for raw materials and reducing agents, large research effort has been spent worldwide to understand and control such complex system. This fact is reflected that many blast furnace mechanistic models[1,2] and model-based controller[3,4] have been constructed during the past decades. Although progress in the development of modeling and control techniques of the blast furnace system has been achieved, these purely mechanistic models can seldom yield successful application in practice due to the following reasons: (a) weak real time

Correspondence concerning this article should be addressed to C. Gao at gaochou@zju.edu.cn.

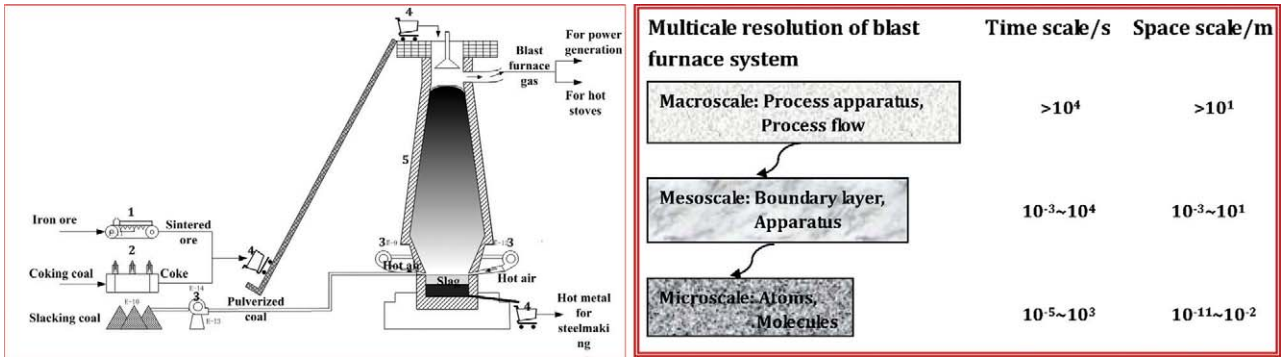

Figure 1. Spatio-temporal multiscale resolution of the blast furnace system.

Left side panel: the flow chart of the blast furnace system. (1) Sintering machine; (2) coke oven; (3) blower; (4) skip car; (5) blast furnace. Right side panel: an approximate multiscale resolution of the blast furnace system. [Color figure can be viewed in the online issue, which is available at wileyonlinelibrary.com.]

performance; (b) excessive assumptions and simplification; (c) difficulty in obtaining the analytical solutions of equations; and (d) very expensive and time-consuming to be constructed. As a complementary method, data-driven modeling is being broadly investigated[5–8] and exhibits great potential for describing the complex behavior of the blast furnace system. In addition, rule-based expert system has also been applied for the blast furnace control by some researchers.[9] However, the complexity of the blast furnace system still forms the main obstacle for realizing the blast furnace automation. Today, experience and intuition of the operators are still the main resort for controlling the blast furnace. A new means of modeling and control for the blast furnace system need be developed to throw more light on overcoming this hurdle.

The purpose of the blast furnace—a huge countercurrent reactor and heat exchanger in steel manufacturing, is to produce molten iron, also called hot metal, from ore. Solid iron ore and coke are charged layer by layer into the top of the furnace, while preheated air with possible additives are blasted through tuyeres located near the bottom of the furnace. The in-furnace process chemistry, multiphase interaction together with the operating condition of high temperature, high pressure and existence of packed particles, lead to the dynamics of the blast furnace system exhibiting the features of strong nonlinearity[10] and nonstationarity.[11] Additionally, some control actions taken in the operation of the blast furnace, such as the adjustment of blast volume, tuyeres diameter, burden distribution and pulverized coal injection, etc., will make the dynamics identification further complicated, since these control actions are usually taken as nonstationary external noise that can camouflage the nonlinearity of the blast furnace system.[11] More importantly, the great difference in the average residence time of solid, liquid and gaseous phase, such as 5 to 10 h for the iron ore and liquid phase, 10 to 20 s for the gaseous phase and 1 to 4 or more weeks for the coke in the hearth, implies that the blast furnace process dynamics occurs at different characteristic times, i.e., multiscale nature.[12] Motivated by the work of Li and Kwauk[13] and Kwauk and Li[14] in chemical engineering field, a kind of approximate multiscale resolution of the blast furnace system with three sublevel structures is illustrated in Figure 1. It is very crucial to diagnose and understand such complex multiscale nature for developing a reliable blast furnace mathematical model. However, the traditional analysis methods based on the idea of average at a fixed scale fail to address the multiscale structure of the blast furnace system. In this regard, multiscale method seems to be able to offer an exciting possibility for describing complex blast furnace dynamics. Thus, the current work is devoted to identifying the multiscale nature and the dynamics of the blast furnace system in the hope of throwing more light on characterizing it.

The remainder of this article is organized as follows: in the next section, the operating data used in this paper is presented, including data acquisition and data preprocessing. This is followed by the identification of multiscale nature and multiple dynamics of the blast furnace system through nonlinear time series analysis. Finally, conclusions and points of possible future research are summarized.

Data Acquisition and Preprocessing

The development of nonlinear science indicates that the dynamics of a system can be addressed by analyzing the time series of any variable of the studied system,[15] so the diagnosis of the blast furnace dynamics may be realized by analyzing the time series of the output variables of the blast furnace system. Among the output variables of the blast furnace system, hot metal temperature and hot metal compositions, such as silicon content (Si, wt %) and sulfur content (S, wt %) in hot metal, are the important parameters for indicating the hot metal quality and the stability of the blast furnace operation, and thus need to be strictly controlled around the set points. The control of the blast furnace operation often means to control these parameters within proper bounds. Because of extremely high temperature in the ironmaking blast furnace, the highest temperature approaching 2000°C, it is very difficult to directly measure the physical temperature of hot metal. Instead, the silicon content in hot metal, often called "chemical temperature of hot metal," is taken as the chief indicator of in-furnace thermal state. Therefore, the time series of the silicon content in hot metal, denoted by y_1, and of the sulfur content in hot metal,

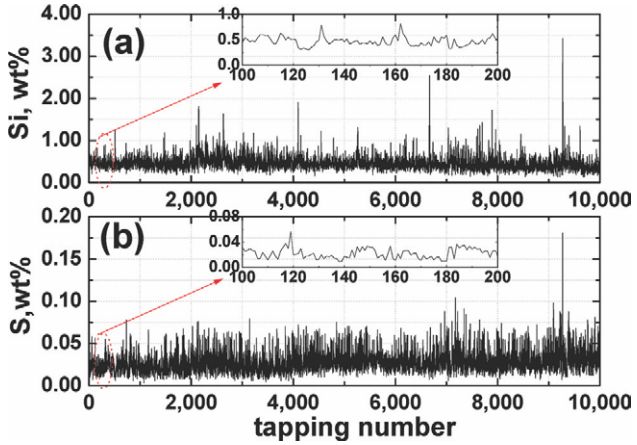

Figure 2. Time series of silicon content (a) and sulfur content (b) in hot metal measured from the selected blast furnace.

[Color figure can be viewed in the online issue, which is available at wileyonlinelibrary.com.]

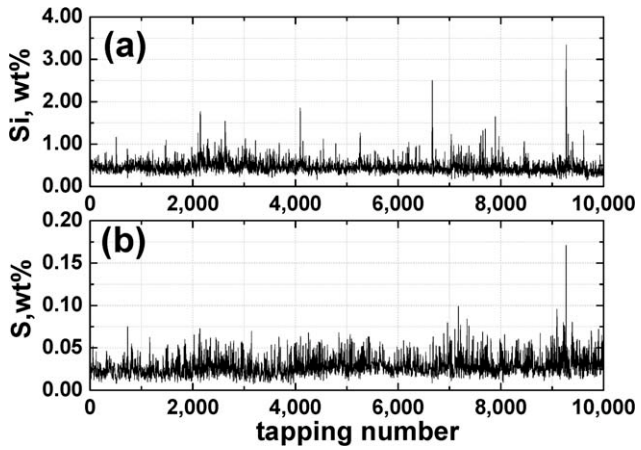

Figure 3. Filtered time series of silicon content (a) and sulfur content (b) in hot metal.

denoted by y_2, are used for identifying the multiscale nature and dynamics of the blast furnace system in this context.

For this study, the time series of the silicon content and sulfur content in hot metal are collected from a pint-sized blast furnace whose working volume is about 750 m^3. Figure 2 illustrates the silicon time series and sulfur time series measured from the selected blast furnace. The size of the records is 10,000, and the sampling frequency is $\sim$0.5 h^{-1}. The depicted silicon and sulfur values are measured through a ladle-wise analysis, a frequently used way to perform chemical components analysis in metallurgical field, through which a test ingot sample is taken from part of the heat during the pouring of the hot metal and then sent to the laboratory for chemical analysis. The reported 10,000 records in Figure 2 are not the analysis results of 10,000 ladles but the ones of 10,000 heats of molten iron, and the sampling frequency of approximate 0.5 h^{-1} indicates about 12 heats of molten iron cast every day. During each tapping, two samples need to be taken and the time instance for ladle analysis is set as follows: one sample is taken at the time the volume of the hot metal occupies one-third of the ladle's volume, the other is taken when the volume of the hot metal occupies two-thirds of the ladle's volume. The whole tap durations are about 35 min. The arithmetical mean of these two analysis results acts as the final result of this heat of molten iron, exhibited in Figure 2. At this point, the above sampling for analyzing hot metal composition is actually a nonuniform sampling. There are other means to set time instance for ladle analysis, such as uniformly distributing the ladle analysis for a tap over the tapping time, and the way jointly taking into consideration the effect of the time lag between producing and tapping the hot metal,[16] etc. Seen from Figure 2, there are strong oscillating behaviors in these two groups of time series, even though an apparent short-term cycle may be observed, i.e., self-similarity. Also it could be observed that there are many spikes contained in both time series, which maybe results from noise. As the realistic measurements, the blast furnace data, particularly the silicon and sulfur transfer data, are expected to be associated with a significant amount of noise, such as process noise and measurement noise. The presence of noise will make the time series quite different from their natural values and may further lead to misleading results in diagnosing the dynamics of the blast furnace system. Thus, we need to reduce noise in the data sets. Here, a wavelet soft thresholding filter[17] is used to tackle the problem. This de-noising technique proceeds in three steps:[17] (1) perform the wavelet decomposition of the studied signal; (2) apply soft thresholding to the detail coefficients; (3) reconstruct the de-noising signal based on the original approximation coefficients and the modified detail coefficients. Figure 3 displays the filtered series. Compared with the original series in Figure 2, the "spikes" phenomena in the filtered series are weakened greatly but without loss of natural shape of the original series. Table 1 presents the statistics of the original series and the filtered series. It can be observed that the distributions of the original silicon and sulfur series are heavy tailed, right skewness, and peaked, while for the filtered data sets, the same distribution property remains but with the standard deviation reduced slightly and the Skew and Kurtosis increased slightly. To observe the distribution of the filtered silicon and sulfur series more carefully, Figure 4 exhibits the histogram of the observed frequencies of occurrence of the filtered silicon and sulfur sequences. Clearly, there are still light right tailed, right skewness and peakness in the distribution of both filtered data sets. For the filtered

Table 1. Statistics of Silicon Time Series and Sulfur Time Series from the Selected Blast Furnace

	Original Time Series		Filtered Time Series	
Statistical Property	Silicon	Sulfur	Silicon	Sulfur
Minimum value	0.130	0.003	0.139	0.007
Maximum value	3.420	0.181	3.341	0.171
Mean	0.455	0.028	0.455	0.028
Standard Deviation(SD)	0.162	0.012	0.147	0.010
Interquartile range IQR)	−0.140	−0.012	−0.091	−0.011
Pseudo SD	−0.104	−0.009	−0.068	−0.008
Coefficient of variability	0.357	0.436	0.323	0.364
Skew	3.624	1.406	4.392	1.561
Kurtosis	33.066	4.741	44.985	6.869

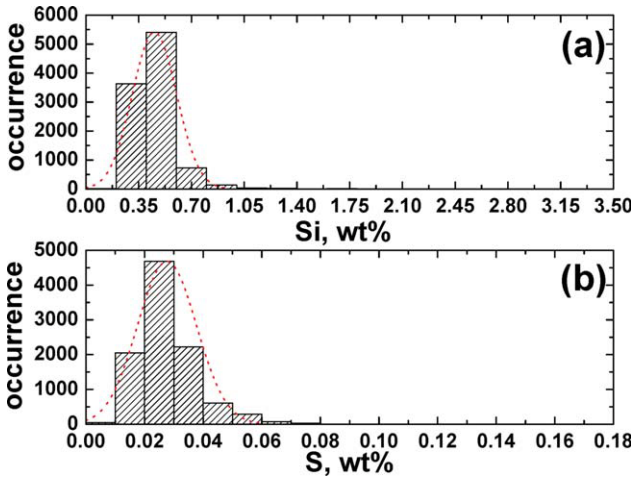

Figure 4. Histogram of the observed frequencies of occurrence of the filtered silicon series (a) and sulfur series (b).

[Color figure can be viewed in the online issue, which is available at wileyonlinelibrary.com.]

silicon series, most data points lie in the range [0.2,0.6], while for the filtered sulfur series, most data points lie in [0.01,0.04].

Identification and Discussion

Hilbert-Huang transform

As the essence of multiscale structure, the nonlinearity and nonstationarity exhibited by the studied silicon and sulfur time series mean it an arduous task to characterize the dynamics of the blast furnace system through traditional techniques based on the idea of average at a fixed scale.[18] For this reason, an analysis of multiscale resolution should be performed on the studied series to identify the multiscale nature of the blast furnace system and give rise to more possibility to capture its dynamics. Among the methods used for multiscale resolution, Hilbert-Huang transform technique[19] is a Hilbert transform based method and has local and adaptive properties. Compared with other multiscale resolution methods, such as wavelet technique that is a linear analysis in essence, Hilbert-Huang transform is more powerful in dealing with nonlinear and nonstationary signals.

There are two main steps to perform multiscale analysis using Hilbert-Huang transform; one is empirical mode decomposition (EMD) and the other is Hilbert transform.[19] EMD is a method to decompose the signals into a number of intrinsic mode functions (IMFs) by sifting out the innate undulations belonging to different time scales. For the studied signal $\{y(k)\}_{k=1}^{N_{\text{dat}}}$, the sifting process can decompose it to be

$$\left\{ y(k) = \sum_{j=1}^{N} C_j(k) + r_N(k) \right\}_{k=1}^{N_{\text{dat}}} \tag{1}$$

where N is the number of time scales, $\{C_j(k)\}_{k=1}^{N_{\text{dat}}}$ represents the jth IMF and $\{r_N(k)\}_{k=1}^{N_{\text{dat}}}$ is the residual term. The second step is the Hilbert transform of IMFs. Hilbert transform is a kind of time-frequency analysis method and can act as a way to derive the analytic signal of a real signal. For the above resolved IMFs, $\{C_j(k)\}_{k=1}^{N_{\text{dat}}}$, $j = 1,\ldots,N$, their analytic signal, $\{\psi_j(k)\}_{k=1}^{N_{\text{dat}}}$, are defined as

$$\psi_j(k) = C_j(k) + \mathrm{i}\widehat{C}_j(k) = A_j(k)e^{\mathrm{i}\phi_j(k)}, j = 1, \ldots, N \tag{2}$$

Here, $\widehat{C}_j(k)$ is the Hilbert transform of $C_j(k)$, $A_j(k)$ are the amplitude and $\phi_j(k)$ are the phase angle. Finally, the instantaneous frequency $\omega_j(\cdot)$ and further the Hilbert spectrum of each IMF component can be achieved by computing the derivative of the phase angle and plotting the frequency-time distribution of the amplitudes, respectively.

Multiscale resolution of the filtered silicon and sulfur signals

For the filtered silicon and sulfur signals, EMD method is performed on them with the results shown in Figures 5 and 6.

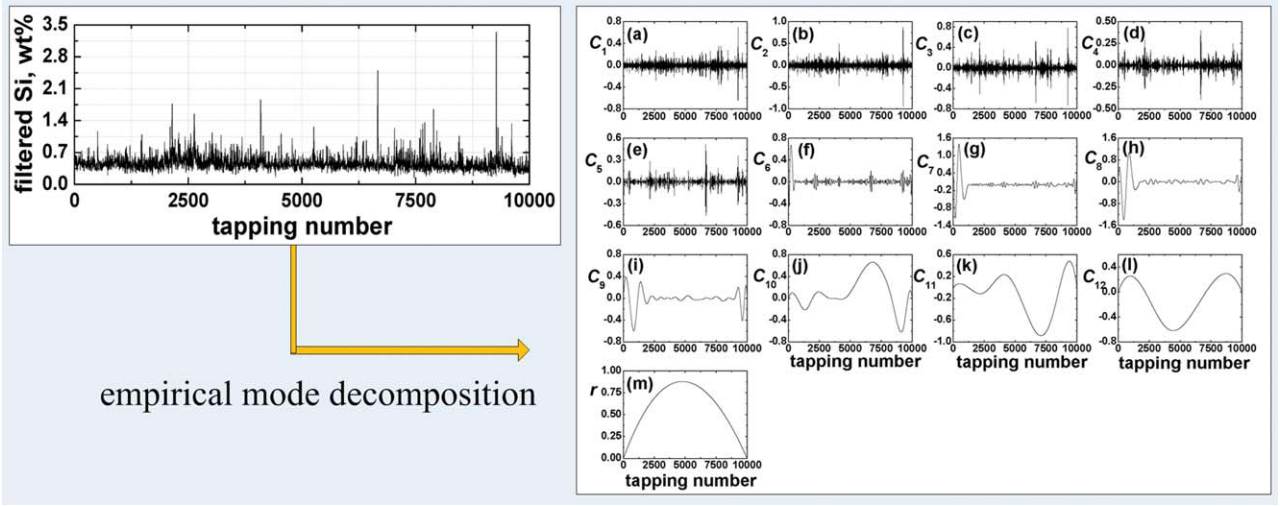

Figure 5. EMD of the filtered silicon recordings, 12 IMFs, C_j (j = 1–12), and the residual r.

[Color figure can be viewed in the online issue, which is available at wileyonlinelibrary.com.]

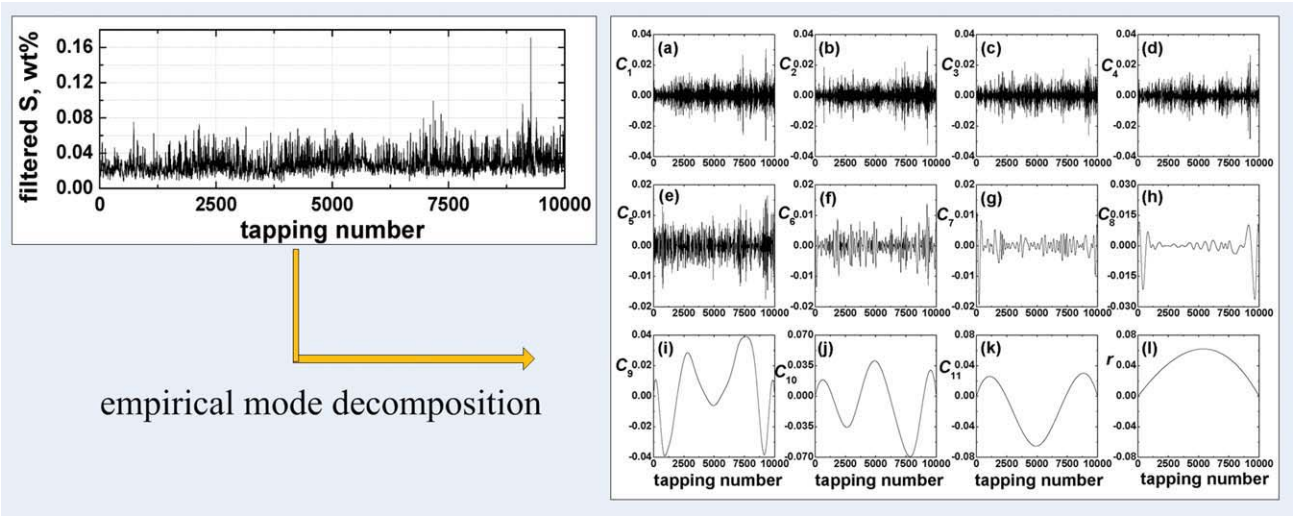

Figure 6. EMD of the filtered sulfur recordings, 11 IMFs, C_j (j = 1–11), and the residual r.

[Color figure can be viewed in the online issue, which is available at wileyonlinelibrary.com.]

Obviously, there are 12 and 11 IMFs resolved from the filtered silicon and sulfur signals, respectively, and the decomposed signals tend to change regularly as j increases even though large oscillations are present in the first seven components. These large oscillations, such as high-frequency changes in IMF 1, may result from the control actions taken during measurements, the behavior of the staff in different shifts or short-term fluctuations in the energy reserve of the process. More detailed analysis on the IMF 1 will be made at a later time. While for the longer-term variations in IMFs 6 and 7, they maybe result from the structure changes in the internal conditions, for example, increased and decreased permeability of the dead man.[20] Also, it should be mentioned that the numbers of IMFs of the two groups of series are slightly different, more time scales emerging in the filtered silicon series. According to the EMD method, the number of IMFs extracted from original series relies on the experimental conditions and the stopping threshold, denoted as ε here.[19] When the experimental conditions are decided, the value of ε will have an effect on the decomposed results. Huang et al.[19] advocated to set ε in the range 0.2–0.3. In the studied silicon and sulfur cases, the number of IMFs is not sensitive to ε, so ε is set to be a typical value 0.2. The difference in the numbers of IMF component contained in the filtered silicon and sulfur series indicates that there are more causes ruling the silicon evolution than the sulfur evolution in the blast furnace system, and larger difficulty may be encountered in predicting silicon than predicting sulfur. The higher complexity of the silicon series could be due to the fact that the sulfur content of hot metal is largely governed by slag basicity and, possibly, by the hot metal carbon content. Also, this difference may lead to difficulty in modeling the blast furnace system according to every sublevel structure, since at some sublevel structures the information of some variables may be scarce, such as sulfur information being scarce at the twelfth subscale. A possible way to solve this problem is to set sulfur variable as zero at this subscale when modeling. Other possible ways for multiscale modeling will be discussed later.

To deepen the analysis of the characteristics hidden in every IMF component of the filtered silicon and sulfur signals, Hilbert transform is carried out on them, and then phase angles corresponding to every IMF component are calculated with the results exhibited as a function of tapping number in Figure 7. Seen from Figure 7, there is an apparent separation between the phase angle plots when $1 \leq j \leq 7$, and their average slops, i.e., the mean instantaneous frequencies $\langle \omega_j \rangle$, decrease rapidly as the order of IMFs increases , nearly to be zero when j reaches 8 for both silicon and sulfur cases. This indicates that the eighth IMF and up can be considered to have approximate zero mean instantaneous frequencies. These low frequency parts, related to larger scale structures, change steadily and regularly as shown in Figures 5 and 6, which further implies that general less sophisticated averaging methods may be enough to deal with them.[21] The detailed average instantaneous frequencies and the relative

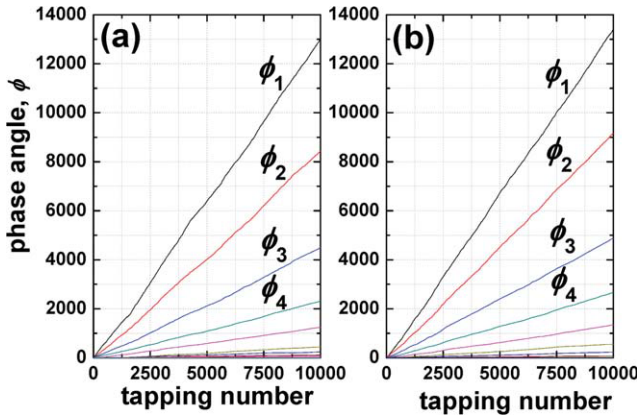

Figure 7. Phase angle ϕ_j vs. tapping number obtained from every IMF component C_j of (a) the filtered silicon time series for j = 1,...,12 and (b) the filtered sulfur time series for j = 1,...,11.

[Color figure can be viewed in the online issue, which is available at wileyonlinelibrary.com.]

Table 2. Mean Instantaneous Frequencies of the First seven IMFs Involved in the Filtered Silicon and Sulfur Series

IMF Components	Silicon Series		Sulfur Series	
	$\langle\omega_j\rangle$ (h^{-1})	Ratio	$\langle\omega_j\rangle$ (h^{-1})	Ratio
C_1	0.655	$\langle\omega_1\rangle$	0.673	$\langle\omega_1\rangle$
C_2	0.425	$\langle\omega_2\rangle$	0.463	$\langle\omega_1\rangle$
C_3	0.226	$\approx\langle\omega_2\rangle/2$	0.246	$\approx\langle\omega_2\rangle/2$
C_4	0.116	$\approx\langle\omega_2\rangle/4$	0.134	$\approx\langle\omega_2\rangle/4$
C_5	0.063	$\approx\langle\omega_2\rangle/8$	0.067	$\approx\langle\omega_2\rangle/8$
C_6	0.025	$\approx\langle\omega_2\rangle/16$	0.030	$\approx\langle\omega_2\rangle/16$
C_7	0.013	$\approx\langle\omega_2\rangle/32$	0.012	$\approx\langle\omega_2\rangle/32$

ratios of the first seven IMFs contained in the filtered silicon and sulfur series are illustrated in Table 2. Since the sampling interval of two groups of series is about 2 h, the results listed in Table 2 are the average slopes of the phase angle plots divided by 2. Here, every mean instantaneous frequency is representative of a physical time scale hidden in the filtered series which can guide the future analysis on what dynamical level,[21] and the signal on every sublevel corresponds to the information produced by every subscale system. A further look at Table 2 suggests that there are only two fundamental frequencies, i.e., $\langle\omega_1\rangle$ and $\langle\omega_2\rangle$, ruling the phase dynamics of the silicon and sulfur signals, since other frequencies can be approximately obtained from $\langle\omega_2\rangle$ by second power decline as the order of IMFs increases. Furthermore, these two average instantaneous frequencies and their distribution along the order of IMFs are nearly the same for the silicon and sulfur series, which means the phase dynamics of the blast furnace system are not as difficult as expected.[7] If an appropriate analytic tool is adopted, such as multiscale method, some common features between the physical variables involved in the blast furnace system can be detected. These common features may be utilized to simplify the description of the blast furnace system dynamics. Therefore, it is possible or may be relatively simple to quantify the dynamics of the blast furnace system from the viewpoint of multiscale. However, it should also be noted that in Table 2 the frequencies $\langle\omega_1\rangle$ and $\langle\omega_2\rangle$ of the first two IMF components are greater than the sampling frequency 0.5 h^{-1}, which obviously infract the well-known Nyquist sampling theorem asserting that a signal bandlimited to B Hz can be recovered by giving its ordinate at a series of points sampled higher than or equal to 2B Hz. Accordingly, based on the Nyquist sampling theorem, the studied silicon and sulfur times series cannot provide reliable frequency information above 0.25 h^{-1}. The obtained frequency information seems beyond the sensitivity of the measurement technique and the sampling rate used.[22] Despite receiving widespread application, it should be pointed out that Nyquist sampling theorem demands uniform sampling in principle, and in addition it only provides a sufficient condition, but not a necessary one, for complete reconstruction. There are many cases beyond Nyquist sampling theorem, such as for sparse (or compressible) bandlimited signals.[23,24] Some empirical results about the sampling rate needed for recover a sparse signal are presented, for example, Tropp et al.[23] reported that the sampling rate R (Hz) satisfies

$$R \approx 1.7K \log\left(W/K + 1\right) \tag{3}$$

where K stands for the sparsity level and W (Hz) is the Nyquist rate, i.e., the band limit. For the studied silicon and sulfur time series, firstly they are obtained by nonuniform sampling, as stated in the previous section; secondly, there are only two fundamental frequencies, i.e., $\langle\omega_1\rangle$ and $\langle\omega_2\rangle$, relative to the band limit. Therefore, the studied silicon and sulfur series can be thought as sparse bandlimited signals with the sparsity level 2, and Eq. 3 will be used to account for the frequency analysis results in Table 2. Substituting the sampling frequency 0.5 h^{-1} and the sparsity level 2 into Eq. 3 can give the maximum frequency information to be 0.677 h^{-1}, which is a little higher than the maximum frequency 0.673 h^{-1} in Table 2. Hence, there is reason to believe that the studied silicon and sulfur series, sampled with the frequency 0.5 h^{-1}, can capture dynamics that takes place at very different time scale, such as at the frequency 0.673 h^{-1}. Namely, the results in Table 2 are believable.

A further look at Table 2 and the scale division in Figure 1 may suggest that the first two components resolved from the filtered series belong to the mesoscale structures of the blast furnace system since the corresponding time scales have the magnitude of 10^3 s, while the remainder components are involved in the macroscale structures. Here, it is worth to mention that the studied silicon and sulfur series cannot capture the microscale dynamics of atoms and molecular in the blast furnace system due to their low sampling frequencies. The contribution of every decomposed component to the whole series may be evaluated by their energy distribution. For a digitized signal, its energy is defined as the squared sum of its amplitude,[25] i.e.,

$$W = \sum_{i=1}^{N_{\text{dat}}} |y(i)|^2 \tag{4}$$

Let $W_j (j = 1,2,\ldots)$ represent the energy of every resolved components from the filtered silicon and sulfur series, then the energy distribution can be expressed as the ratio of energy at different sublevels to the total energy

$$R_j = \frac{W_j}{\sum_j W_j} \times 100\% \tag{5}$$

Shown in Table 3 are the results of the energy distribution. Clearly, in the range of the current frequency information captured by the silicon and sulfur signals, over 99% energy is concentrated in the macroscale structures of the blast furnace

Table 3. Energy Distribution (%) of Every Discomposed Component of the Filtered Silicon and Sulfur Series

Scale		Silicon		Sulfur	
Meso-	C_1	0.88%	0.35%	0.74%	0.37%
	C_2		0.53%		0.37%
Macro-	C_3	99.12%	0.60%	99.26%	0.39%
	C_4		0.29%		0.40%
	C_5		0. 40%		0.32%
	C_6		0.96%		0.25%
	C_7		6.08%		0.19%
	C_8		7.89%		0.66%
	C_9		2.32%		10.03%
	C_{10}		10.60%		21.28%
	C_{11}		16.11%		24.30%
	C_{12}		11.32%		–
	r		42.55%		41.44%

system while little energy is distributed in the mesoscale structures. As a result, the dynamics of the macroscale structure of the blast furnace system is dominant in all dynamics present in the blast furnace system. More attention should be placed on this part for the future modeling, control and optimization purposes, which in turn indicates that the used analytic methods are convincing since most of the efforts in the blast furnace modeling so far has already been on the macroscale. However, even so, it still poses a great challenge to investigate the macroscale structure since it still includes multiple sublevel structures.

Dynamic analysis of the resolved components of the filtered silicon and sulfur series

In the early work,[7,26] a detailed analysis on the blast furnace dynamics was made, and a deterministic component but not completely deterministic mechanism was found to rule the blast furnace dynamics. Based on these studies, a purely chaos-based predictor was constructed to predict the silicon content in the blast furnace hot metal.[7] Since chaotic mechanism is just one of mechanisms ruling the blast furnace dynamics, the purely chaotic predictor is inadequate to follow the evolution of silicon content. This fact is reflected in achieving good but not perfect silicon prediction using the established purely chaotic predictor.[7] However, the traditional methods fail to identify the multiple dynamics at different scale and are also unable to separate the deterministic component from the whole signal, so it is impossible to build a multiple model for silicon prediction following the existent mechanisms in the blast furnace dynamics. Now it becomes possible to identify the multiple dynamics ruling the blast furnace system at different time scale and establish a multiple model for silicon prediction. The complicated silicon and sulfur series, characterized by strong oscillating behavior and many local extremum points, are decomposed into 12 and 11 IMFs, respectively, through multiscale analysis. Dynamic analysis may be performed on these well-behaved IMFs to identify the present dynamics at different time scale of the blast furnace system, i.e., to determine the dynamical behavior of every IMF component to be regular, chaotic or random. Of course, it should be with great caution to combine the EMD decomposition with traditional nonlinear measures, since the complex structure of the IMFs makes it very difficult to extract either qualitative or quantitative information about the underlying dynamics by applying the phase space embedding technique.[27] Although the effects of the EMD decomposition on the time-correlation features of the time series can be negligible,[21] traditional nonlinear measures such as maximum Lyapunov exponent (MLE), correlation dimension etc. may sometimes fail to decide the dynamics of these time series after performing EMD decomposition. In that case, more sophisticated analysis, such as phase-space dissimilarity measures,[28] may be needed, which can quantify dynamical changes in nonlinear, possibly chaotic, processes.

Lyapunov exponents, measuring the averaged divergence or convergence rate of nearby orbits in phase space of a dynamical system, are often thought as the most striking indicator to characterize system dynamics. For a dynamical system, the number of Lyapunov exponents is equal to the number of dimensions of the phase space. Among all the Lyapunov exponents, the MLE, denoted as λ_1, is the most concerned, since it can represent different type of motion of system, with $\lambda_1 < 0$ indicating stable fixed point; $\lambda_1 = 0$ stable limit cycle; $0 < \lambda_1 < \infty$ chaos and $\lambda_1 = \infty$ randomicity.[29] Compared with other indicators of chaos, such as correlation dimension, Kolmogonov entropy, the MLE can provide more information on orbital instabilities. There are many algorithms reported in the literature[30–32] to estimate the Lyapunov exponents from a time series, most of which are based on reconstruction of the phase space.[33] However, these algorithms usually fail to compute the Lyapunov exponents of experimental noisy time series, especially for those obtained from the ladle analysis. Although the noise reduction of the original silicon and sulfur sequences are performed prior EMD decomposition, there are probably still noise in the filtered series and thus in the decomposed components. To weaken the effect of the noise on the computation of Lyapunov exponents, a robust method[34] to estimate the MLE is used in the subsequent investigation, which not only has the robustness over noise but does not depend explicitly on the correct reconstructed parameters.

Before computing the MLE of every resolved component of the silicon and sulfur recordings, the reconstructed parameters, i.e., delay time τ and embedding dimension d, of every decomposed component should be determined first. These two parameters reflect important information on the real system that produces the studied time series. Delay time describes how long the dynamical information can be preserved between the points while embedding dimension indicates the number of actual process variables needed to model the system. There exist a lot of methods for determining these parameters, such as autocorrelation function,[35] mutual information[36] for delay time, and false neighbors,[37] improved false neighbors[38] for embedding dimension. Thereinto, mutual information technique has superior performance in measuring a more general relationship including linearity and nonlinearity contained in a time series, and under some conditions, it can be effectively used to elucidate the deterministic nature of a series.[36] Thus, mutual information technique is used to estimate delay time in the current work. The improved false neighbors method is used to decide embedding dimension since it can avoid selecting the threshold values with subjectivity needed in false neighbors technique and also can distinguish deterministic signal from stochastic signal.[38] Here, to avoid the biased phase space analysis produced by EMD process, the effect of the EMD process on the persistence of the resulting IMFs is analyzed using mutual information function. Figure 8 displays the corresponding results of the silicon and sulfur series and their first three decomposed IMFs. The curves of the mutual information functions for the other IMFs are omitted since they are all located over the curves of the corresponding original signals. Clearly, as Briongos et al.[21,27] pointed out, the time correlation induced by EMD process is almost negligible. Therefore, the influence of the EMD process on the subsequent phase space analysis is almost negligible.

Table 4 gives the results of the reconstructed parameters of every resolved component of the silicon and sulfur signals. It is evident that there is no finite embedding dimension for the first IMF components, C_1 of the silicon and sulfur

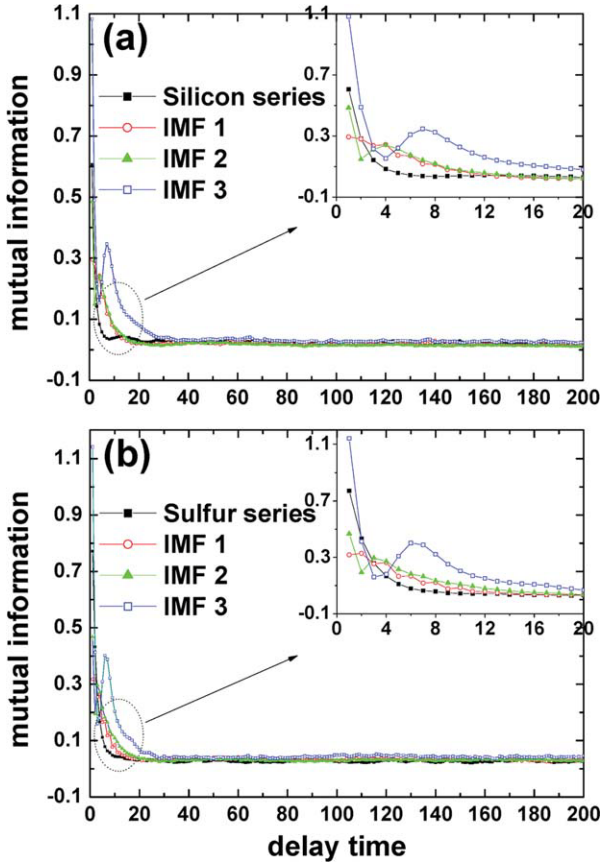

Figure 8. Mutual information function of the filtered silicon series (a) and the filtered sulfur series (b) and their first three IMFs.

[Color figure can be viewed in the online issue, which is available at wileyonlinelibrary.com.]

series. This phenomenon rends strong indication of random behavior in the first IMF components of the silicon and sulfur series, which is consistent with that the random component of data is mainly included in the first IMF through EMD process.[39] Conversely, the above result also indicates that the external disturbance, such as control actions taken during measurements, the behavior of the staff in different shifts or short-term fluctuations in the energy reserve of the process, etc., will have almost no effect on the dynamics of other IMF components. For the random behavior appearing in the IMF 1, there are three possibilities to produce it. The first possibility is that there is inherent random dynamics ruling the evolvement of the silicon and sulfur series; the second one is that the residual process noise and measurement noise appear in the C_1 since it is difficult to filter noise completely from a real data; while the third one comes from the blast furnace control actions taken during measurements, the behavior of the staff in different shifts or short-term fluctuations in the energy reserve of the process, which are viewed as external noise that can camouflage the randomicity.[11] As far as the studied silicon and sulfur recordings are concerned, the time of their measurements last for more than 2 years, so it is taken for granted that there are many blast furnace control actions taken during this period. Despite being filtered partly, it is still highly possible that the adopted blast furnace control actions result in the random component in the silicon and sulfur series. Some simulation experiments may be needed to reveal the truth. Here, it should be with caution to account for the present random behavior in IMF 1 of two groups of time series. However, whatever the possible reason is, for this random part some random theories and methods may be directly applied to obtain more information. In the meantime, the following information is clear from Table 4: (i) Among IMFs 2–9, the delay time increase gradually as the order of IMFs increase for both silicon and sulfur cases. Since larger delay time usually means longer time the dynamical relationship can be preserved, this result indicate that the information of smaller scale structures will lose faster than that of larger scale ones. Thus smaller scale structures in the blast furnace system have more complex dynamics than larger scale ones, i.e., the mesoscale structures of blast furnace system are more complex than the macroscale structures. As to the exceptions taking place in the first, the tenth, the last IMFs, and the residual, the possible reasons may be that: (a) C_1 is a nearly complete random series and mutual information technique is not a good candidate to determine the delay time.[36] The delay time result of C_1 is not illustrative to explain complexity. (b) There may be dynamics change from IMF 9 to IMF 10. (c) The edge effects of the data points result in a drop of delay times in the last IMFs of the silicon and sulfur signals compared with the previous IMFs.[35] (d) The residual is not an IMF and thus it is improper to evaluate its complexity with that of an IMF using the same criterion. (ii) Larger scale structures have lower (at most the same) embedding dimensions than smaller scale structures except the fourth IMF in the sulfur series case. This result indicates that more (at least the same) physical variables are needed to capture the dynamics of smaller scale structures of the blast furnace system, i.e., mesoscale structures of the blast furnace system are higher dimensional subsystems and can be thought to be more complex than macroscale subsystems. Furthermore, although there is a very high embedding dimension appearing in the fourth IMF, the embedding dimensions of all IMFs are lower than the practical number of physical variables of the blast furnace model based on the traditional average methods at a single scale, such as 20 variables reported by Bhattacharya,[5] 15 variables reported by Saxén and Pettersson[6] and 18 variables reported by Gao et al.[7] Namely, a high dimensional blast furnace system is decomposed into a few relative low

Table 4. Reconstructed Parameters (RP) of the Decomposed Components of the Filtered Silicon and Sulfur Series

Series	RP	C_1	C_2	C_3	C_4	C_5	C_6	C_7	C_8	C_9	C_{10}	C_{11}	C_{12}	r
Silicon	τ	3	2	4	7	14	30	50	93	128	101	133	73	117
	d	–	10	10	10	8	5	4	4	3	3	3	3	2
Sulfur	τ	3	2	3	6	12	29	62	125	130	68	75	–	136
	d	–	10	10	12	8	5	5	3	3	3	3	–	2

Table 5. Maximum Lyapunov Exponent of Every Component Resolved from the Filtered Silicon and Sulfur Series

Series	C_1	C_2	C_3	C_4	C_5	C_6	C_7
Silicon	∞	0.001	0.002	0.012	0.013	0.013	0.007
Sulfur	∞	0.001	0.002	0.007	0.022	0.010	0.001
Series	C_8	C_9	C_{10}	C_{11}	C_{12}	r	
Silicon	0.002	0.002	0.000	0.000	0.000	−0.000	
Sulfur	0.003	0.000	0.000	0.000	–	−0.000	

dimensional subsystems. In this regard, the complexity of the blast furnace system is reduced using the multiscale analysis methods. However, the above analysis cannot provide any information on the candidate actual variables for every sublevel scale. Due to the difference in the embedding dimension of different subscale, the same blast furnace process variables, such as coke rate, blast temperature, etc., may have different contribution to the different sublevel structure. Other methods, such as principal component analysis, partial least square, expert experiences, and some reported results,[5,6] are needed to identify the candidate variables. A feasible strategy is to analyze the relationship between the actual blast furnace variables and the output information in every subscale structure according to the corresponding embedding dimension. (iii) For the first six IMFs of the silicon and sulfur signals, both silicon and sulfur cases have the approximately equal delay time and embedding dimension at the same order of IMF. The property of this result is consistent with that of Hilbert transform analysis where almost the same mean instantaneous frequencies are found at the same order of IMF for the first six IMFs of the silicon and sulfur series. This in turn proves that multiscale resolution of the blast furnace system is effective and some inherent characteristics hidden in time series can be explored through scales decomposition. However, from the seventh and up IMFs, the delay times are very different between these two groups of series while the embedding dimensions keep the same nearly. The great difference in delay time for these IMFs between two groups of series may result from the different numbers of their sublevel structures. (iv) The delay time of all decomposed components from the silicon series are larger than that of the original silicon series reported in the early paper,[7,26] where $\tau = 1$ is obtained for the silicon series collected from the same blast furnace as used in this work. This result again proves that every decomposed component of the silicon series has lower complexity than the original silicon series, i.e., the whole blast furnace system being representative of the filtered silicon and sulfur series, is more complex than its sublevel systems being representative of the corresponding IMFs.

Some qualitative information about the dynamics of the blast furnace system is obtained from analyzing the results of Table 4. In the following, according to the reconstructed parameters listed in Table 4, the MLE of every component resolved from the silicon and sulfur series is computed to characterize the dynamics of the blast furnace system quantitatively. Table 5 exhibits the results of the MLE of every component decomposed from the filtered silicon and sulfur series. It can be seen that these resolved subscale levels have three kinds of MLE values, ∞ for IMF 1, positive number for IMFs 2 to 9 in silicon case and for IMF 2 to 8 in sulfur case, and approximate zero for the latter components, respectively, indicating that there are three kinds of dynamics, i.e., randomicity, chaos, and limit cycle, ruling the evolution of silicon and sulfur content in the blast furnace hot metal. A further combination of the current results with the two-scale structures of blast furnace system obtained from Table 3 reveals that the mesoscale structure of the blast furnace system may have two kinds of dynamics, i.e., stochastic mechanism and chaotic mechanism, while the macroscale structure of the blast furnace have chaos and limit cycle dynamics. Of course, the stochastic mechanism may be produced by the incompletely filtered noise or the control actions taken during measurements. In a similar manner, these results indicate that the same subscale structure of the blast furnace system may have multiple control mechanisms, which together with the unidentified microscale dynamics in turn implies that the blast furnace system is indeed highly complex. A more careful look at Table 5 may suggest there is a sudden increase of MLEs from IMF 4 to IMF 5 in the sulfur case, i.e., the sudden increase of chaotic extent from IMF 4 to IMF 5. Additionally, it should be noted that despite the possible presence of three kinds of different dynamics in the blast furnace system, their contribution to the whole system are not equal. Given the energy distribution of every subscale structure illustrated in Table 3, limit cycle is the dominant dynamics, chaos is the secondary dynamics and randomicity may be the third dynamics. Thus, a blast furnace system often displays a globally stable but locally unstable behavior on the normal operational conditions. These results may serve to account for the contradiction that there is no significant change in silicon content when some operation parameters of the blast furnace system have been changed slightly (sensitive dependence on initial conditions, which is the inherent feature of chaos), although chaotic behavior is detected in the evolution of the silicon series.[7,26] At the same time, these results can also be used to explain why many models based on different mechanisms can work for the blast furnace system to a certain extent, such as random model,[16] chaotic model,[7] and deterministic model.[2] Additionally, these results can even serve as a guideline for choosing appropriate tools to model, control and optimize the blast furnace system. Namely, a multimodal model that reflects periodical, chaotic, and stochastic features is needed for describing the complex dynamics of the blast furnace system. In the practice, there may be two cases to implement the above task. One case is just to utilize the pure historical records of the silicon/sulfur series, the other case is to augment other measurable variables as inputs which are known to have a correlation on the silicon/sulfur. For the first case, the silicon/sulfur information on every sublevel structure may be directly utilized to modeling in terms of the corresponding mechanism, such as random model for subscale 1 structure, chaotic model for subscale 2 structure, etc. The outputs of every subscale model are integrated to achieve the final output of the silicon/sulfur

content. While for the second case, the blast furnace measurable variables are carried out the same multiscale decomposition as the silicon/sulfur series firstly, then in every sublevel scale, some measurable variables related to the silicon/sulfur content are screened out as inputs based on principal component analysis, partial least squares, expert experiences etc. Finally, every subscale model is constructed according to the corresponding dynamics, and the integration of every subscale model output is taken as the ultimate output. Generally, the second case can yield a more accurate prediction model than the first case. Despite some advantages exhibited by using multiscale methods for analyzing the blast furnace system, like lower complexity and definite dynamic for every subscale structure, there are still many difficulties encountered in the practical modeling of the blast furnace system, such as errors accumulation from multiple models and how to integrate the outputs of every sublevel model, etc. In a word, multiscale modeling for the blast furnace system is quite a difficult and broad issue.

Conclusions and Future Research

In this work, the data sets of two key components in the blast furnace hot metal, i.e., silicon content and sulfur content, collected from a small blast furnace, are analyzed to identify the possible multiscale nature and dynamics of the blast furnace system through combing Hilbert-Huang transform method with some nonlinear time series analysis techniques. The results render strong indication of multiscale structures, 13 sublevel components for the silicon series and 12 sublevel components for the sulfur series, and multiple dynamics, chaos, limit cycle, and possible randomicity, contained in the blast furnace system. However, the contributions of every dynamical mechanism to the whole blast furnace system are not equal. The macroscale structure of the blast furnace system containing chaos and limit cycle dynamics needs to be given special attention in the future research due to its high (99%) energy rate.

The main contribution of the current work is to provide an experimental basis for performing multiscale analysis on the blast furnace system. Future investigations may include modeling of every subscale structure of the blast furnace system and integrating these models; finding proper control strategies to reflect the detected dynamics; investigating the correlation and coupling strength between adjacent subscale structures; augmenting other important variables involved in the blast furnace system, such as some input variables, i.e., blast temperature, blast volume and coke rate, etc., for multiscale resolution; analyzing the effect of the size of the original data sets on the results and applying the current work to other modern large-scale blast furnace, etc. All of these are deemed to be helpful to throw more light on understanding and controlling the blast furnace system. In conclusion, notwithstanding some limitations, the diagnosis of multiscale nature and multiple dynamics of the blast furnace system provide a novel thought to analyze and characterize the blast furnace system.

Acknowledgments

The authors acknowledge the financial contribution of National Natural Science Foundation of China under Grant No. 10901139, 60911130510, and the key project of Zhejiang University of Finance and Economics of China. Thanks are also given to the anonymous reviewers for their many valuable comments.

Literature Cited

1. Takatani K, Inada T, Ujisawa Y. Three-dimensional dynamic simulator for blast furnace. *ISIJ Int*. 1999;39:5–22.
2. Nogami H, Chu MS, Yaji J. Multi-dimensional transient mathematical simulator of blast furnace process based on multi-fluid and kinetic theories. *Comput Chem Eng*. 2005;29:2438–2448.
3. Radhakrishnan VR, Ram KM. Mathematical model for predictive control of the bell-less top charging system of a blast furnace. *J Process Control*. 2001;11:565–586.
4. Takahashi H, Kawai H, Kobayashi M, Fukui T. Two dimensional cold model study on unstable solid descending motion and control in blast furnace operation with low reducing agent rate. *ISIJ Int*. 2005;45:1386–1395.
5. Bhattacharya T. Prediction of silicon content in blast furnace hot metal using Partial Least Squares (PLS). *ISIJ Int*. 2005;45:1943–1945.
6. Saxén H, Pettersson F. Nonlinear prediction of the hot metal silicon content in the blast furnace. *ISIJ Int*. 2007;47:1732–1737.
7. Gao CH, Chen JM, Zeng JS, Liu XY, Sun YX. A chaos-based iterated multistep predictor for blast furnace ironmaking process. *AIChE J*. 2009;55:947–962.
8. Radhakrishnan VR, Mohamed AR. Neural networks for the identification and control of blast furnace hot metal quality. *J Process Control*. 2000;10:509–524.
9. Warren P, Harvey S. *Development and implementation of a generic blast-furnace expert system*. Transactions of the Institution of Mining and Metallurgy Section C-Mineral Processing and Extractive Metallurgy, London, UK. vol. 110, 2001:C43–C49.
10. Waller M, Saxén H. Application of nonlinear time series analysis to the prediction of silicon content of pig iron. *ISIJ Int*. 2002;42:316–318.
11. Miyano T, Kimoto S, Shibuta H, Nakashima K, Ikenaga Y, Aihara K. Time series analysis and prediction on complex dynamical behavior observed in a blast furnace. *Physica D*. 2000;135:305–330.
12. Saxén H, Östermark R. State realization with exogenous variables-a test on blast furnace data. *Eur J Oper Res*. 1996;89:34–52.
13. Li JH, Kwauk M. Exploring complex systems in chemical engineering-the multi-scale methodology. *Chem Eng Sci*. 2003;58:521–535.
14. Kwauk M, Li JH. Three transport and one reaction multi-scale. *Prog Nat Sci*. 2000;10:1078–1082.
15. Takens F. *Detecting strange attractor in fluid turbulence*. In: Rand D, Young LS. *Lecture Notes in Mathematics*, Berlin: Springer, 1981:366–381.
16. Saxén H. Short-term prediction of silicon content in pig iron. *Can Metall Quart*. 1994;33:319–326.
17. Donoho DL. De-noising by soft-thresholding. *IEEE Trans Inf Theory*. 1995;3:613–627.
18. Li JH, Zhang JY, Ge W, Liu XH. Multi-scale methodology for complex systems. *Chem Eng Sci*. 2004;59:1687–1700.
19. Huang NE, Shen Z, Long SR, Wu MD, Shih HH, Zhen Q, Yen NC, Tung CC, Liu HH. The empirical mode decomposition and the Hilbert spectrum for nonlinear and non-stationary time series analysis. *Proc Royal Soc London A*. 1998;454:903–995.
20. Helle M, Saxen H. Data-Driven analysis of sulfur flows and behavior in the blast furnace. *Steel Res Int*. 2008;79:671–677.
21. Briongos JV, Aragon JM, Palancar MC. Phase space structure and multi-resolution analysis of gas-solid fluidized bed hydrodynamics: Part I-The EMD approach. *Chem Eng Sci*. 2006;61:6963–6980.
22. Shimoda K, Saito K. Detailed structure elucidation of the blast furnace slag by molecular dynamics simulation. *ISIJ Int*. 2007;47:1275–1279.
23. Tropp JA, Laska JN, Duarte MF, Romberg JK, Baraniuk RG. Beyond Nyquist: efficient sampling of sparse bandlimited signals. *IEEE Trans Inf Theory*. 2010;56:520–544.
24. Donoho DL. Compressed sensing. *IEEE Trans Inf Theory*. 2006;52:1289–1306.
25. Zhao GB, Yang YR. Multiscale resolution of fluidized-bed pressure fluctuations. *AIChE J*. 2003;49:869–882.
26. Gao CH, Zhou ZM, Chen JM. Assessing the predictability for blast furnace system through nonlinear time series analysis. *Ind Eng Chem Res*. 2008;47:3037–3045.

27. Briongos JV, Aragon JM, Palancar MC. Phase space structure and multi-resolution analysis of gas-solid fluidized bed hydrodynamics: Part II: Dynamic analysis. *Chem Eng Sci*. 2007;62:2865–2879.
28. Hively LM, Protopopescu VA. Machine failure forewarning vi phase-space dissimilarity meausures. *Chaos*. 2004;14:408–419.
29. Kantz H, Schreiber T. *Nonlinear Time Series Analysis*. Beijing: Tsing Univerisity Press, 2001.
30. Wolf A, Swift JB, Swinney LH, Vastano JA. Determining Lyapunov exponent from a time series. *Physica D*. 1985;16:285–317.
31. Eckmann JP, Kamphorst SO, Ruelle D, Ciliberto S. Liapunov exponents from time series. *Phys Rev A*. 1986;34:4971–4979.
32. Sano M, Sawada Y. Measurement of the Lyapunov spectrum from a chaotic time series. *Phys Rev Lett*. 1985;55:1082–1085.
33. Packard NH, Crutchfield JP, Farmer JD, Shaw RS. Geometry from a time series. *Phys Rev Lett*. 1980;45:712–716.
34. Kantz H. A robust method to estimate the maximal Lyapunov exponent of a time series. *Phys Lett A*. 1994;185:77–87.
35. Lai YC, Ye N. Recent developments in chaotic time series analysis. *Int J Bifurcat Chaos*. 2003;13:1383–1422.
36. Fraser AM, Swinney HL. Independent coordinates for strange attractor from mutual information. *Phys Rev A*. 1986;33:1134–1140.
37. Kernel MB, Brown R, Abarbanel HDI. Determining embedding dimension for phase-space reconstruction using a geometrical construction. *Phys Rev A*. 1992;45:3403–3411.
38. Cao LY. Practical method for determining the minimum embedding dimension of a scale time series. *Physica D*. 1997;110:43–50.
39. Franzke C. Multi-scale analysis of teleconnection indices: climate noise and nonlinear trend analysis. *Nonlin Processes Geophys*. 2009;16:65–76.

Manuscript received Apr. 22, 2010, and revision received Dec. 15, 2010.